IOP Conference Series: Earth and Environmental Science

PAPER • OPEN ACCESS

Tectonic Setting of Mount Agung, Bali: Insight From Petrology and Geochemistry Analysis

To cite this article: A Syafitri *et al* 2022 *IOP Conf. Ser.: Earth Environ. Sci.* **1047** 012005

View the article online for updates and enhancements.

You may also like

- Identifying key factors determining dynamics of environmental characteristics in Lesser Sunda island, Indonesia
E D Lusiana, S Astutik, Nurjannah et al.
- Land use cover changes and water quality of Cipunten Agung Watershed Banten
Afifa Karima and Regan Leonardus Kaswanto
- Forecasting the climate response to volcanic eruptions: prediction skill related to stratospheric aerosol forcing
M Ménégoz, R Bilbao, O Bellprat et al.

This content was downloaded from IP address 71.15.255.18 on 16/06/2024 at 15:13

TECTONIC SETTING OF MOUNT AGUNG, BALI: INSIGHT FROM PETROLOGY AND GEOCHEMISTRY ANALYSIS

A Syafitri[1], I G B E Sucipta[2], A N Arifa[1], A Saepuloh[2], and S Widiyantoro[3,4]

[1] Laboratory of SEM-EDS UPP Chevron – Bandung Institute of Technology, Indonesia

[2] Petrology, Volcanology, and Geochemistry Research Group, Geological Engineering, Faculty of Earth Science and Technology – Bandung Institute of Technology, Indonesia

[3] Global Geophysics Research Group, Faculty of Mining and Petroleum Engineering – Bandung Institute of Technology, Indonesia

[4] Faculty of Engineering, Maranatha Christian University, Bandung, Indonesia

Corresponding author: auliasyafitri10@gmail.com

Abstract. One of the longest arcs in the world originated from the complexity of subduction zones is the Sunda Arc that covers 80% of Indonesia's active volcanoes, from the Andaman, Sumatra, Java, and the Lesser Sunda Islands. Previous research in magmatism in Sunda Arc has conceded that the continental crust is in the west and becomes progressively oceanic towards the east. However, recent research has suggested that continental basement is more widespread than previously thought. Therefore, this study aims to re-evaluate the tectonic setting of Mount Agung, Bali, part of the Lesser Sunda Islands. Based on the results of published geochemistry data analysis and our petrological and/or mineralogical data, we found that Mount Agung was influenced by three cogenetic magmas and can be divided into 4 eruption periods, i.e., pre-3200±60 BP, 3200±60 – 1870±40 BP, 1870±40 – 1040±50 BP, and post-1040±50 BP. These calc-alkaline magmas were derived from partial melting caused by the subduction of the Indo-Australian Plate within the Eurasian Plate. It produced basalt to dacite rocks with SiO_2 varying between 51 and 63 wt%. As seen from the spider diagram, Rb, Ba, Th, K, and La – Sm contents are enriched, while Eu – Lu experienced depletion. In addition, the Nb content shows a negative anomaly, which is a characteristic of volcanic products from convergent plate boundaries. Based on the ratio of Zr to Zr/Y, it introduces that Mount Agung is affected by continental arcs. La/Sm to Th/Nb diagram reveals that in the older period (pre-1040±50 BP), the magma differentiation process is subduction-related enrichment, while in the younger period (post-1040±50 BP), there may be a slight influence from the presence of crustal contamination. Thus, these analyses presume that Bali Island has a continental basement (micro-continent basement), which may become the eastern end boundary of Sundaland.

Content from this work may be used under the terms of the Creative Commons Attribution 3.0 licence. Any further distribution of this work must maintain attribution to the author(s) and the title of the work, journal citation and DOI.
Published under licence by IOP Publishing Ltd

1. Introduction

One of the longest arcs in the world originated from the complexity of subduction zones is the Sunda Arc. The Sunda Arc covers up to 80% of Indonesia's active volcanoes from the Andaman Island, Sumatra, Java, and the Lesser Sunda Islands [1, 2]. It was formed by the Indo-Australian Plate subduction under the Eurasian Plate, which has been continuously activated since the Middle Eocene (around 45 Ma) [2, 3, 4]. This arc is very unique because it contains the transition between continental and oceanic-type arcs [2]. However, due to the lack of basement research, it is still unclear, which part is inherited from the oceanic and the continental crust [2]. Previous research in magmatism has conceded that the continental crust is in the west (Sumatra, Java), through the transition (Bali, Lombok), and becomes progressively oceanic towards the east (Wetar, Banda) [5, 6]. However, recent studies have suggested that continental basement is more widespread than previously thought [2, 7, 8].

This paper presents further work in this direction, particularly in searching the area that is still part of the continental basement. Bali Island, as a transition zone, is an intriguing area to debate. Previous research stated that it is derived from volcanic island arc [5, 9, 10], which is originated from subduction between oceanic crusts [11]. Thus, our study aims to re-evaluate the tectonic setting of Bali. This matter can be identified using the geochemical characteristic of volcanic rocks [12, 13]. Thus, one of the active volcanoes in Bali, Mount Agung provides useful information on interpreting the tectonic environment of this island.

2. Geological Background

Sundaland is the continental core of SE Asia [7, 14, 15] (Figure 1). Its eastern margin is irregular; a boundary has often been drawn through West Java, northeast to Borneo, and then northwest towards South China Sea [7]. Nowadays, further east, including East Java, West Sulawesi, and potentially the several small islands towards Flores and Sumba, is underlain by a continental crust that becomes the edge of Sundaland [7]. The basement of Bali may have varying densities and thicknesses that come from the transition between continental and oceanic types, which may be a product of mélange [4, 5, 16]. The basement of western Bali may originate from Argoland (a fragment of the Australian continental crust), whereas the eastern part may be part of a suture zone that extends to Sulawesi [4, 16] (Figure 2).

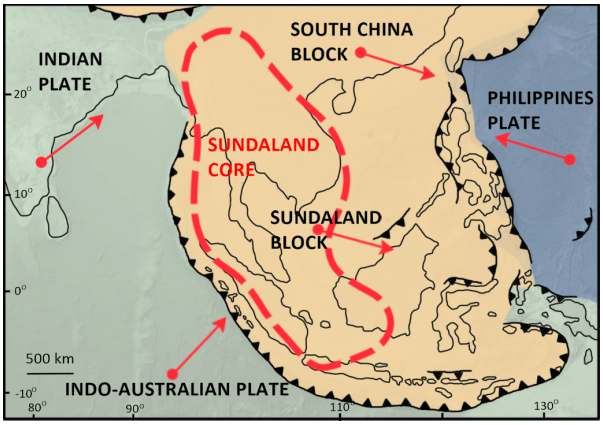

Figure 1. Location of the Sundaland Block as a core in SE Asia [8]. Large arrows represent the direction of plate motions.

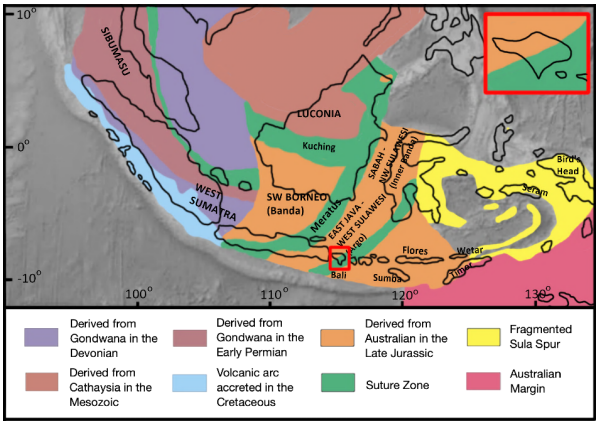

Figure 2. Main arc basement of the Indonesian Crust [7]. Bali Island (shown in box) has a constituent crust originating from the Argoland (a fragment of the Australian Continent Crust in the Late Jurassic Period) in the west and the suture zone in the east [4, 16].

Bali is located in the Lesser Sunda, the eastern part of Sunda Arc, consisting of many small volcanic islands between Java and the Banda Arc (Figure 3). These islands are the product of subduction, collision, and volcanism [16]. The boundary between the Lesser Sunda Islands and the Banda Arc coincides with a change in the present-day plate boundaries between the Indo-Australian and Eurasian plates, from oceanic plate subduction to continental plates collision [16].

The basic stratigraphy of Bali [17, 18] shows that the oldest exposed rock, the Early Miocene Ulakan Formation, is consists of volcanic breccia, lava, and tuff intercalated with carbonate material. Most of the island is covered by Quaternary volcanic deposits originating from the Ancient Volcanoes, Bratan-Batukau-Seraya, and two active volcanoes, Mount Batur and Mount Agung [17, 18]. Mount Agung is situated in eastern Bali. It has one main crater at 3014 meters above sea level. In addition, Mount Agung also has a parasitic cone, Bukit Pawon, on the southeastern slope, with an altitude of 800 meters above sea level. The main crater eruption products consist of 14 lava units, 6 pyroclastic flow units, 3 pyroclastic fall units, and 3 lahars units [19]. Based on the known history, Bukit Pawon only erupted once and produced lava as well as scoria units scattered locally around it [19] (Figure 4).

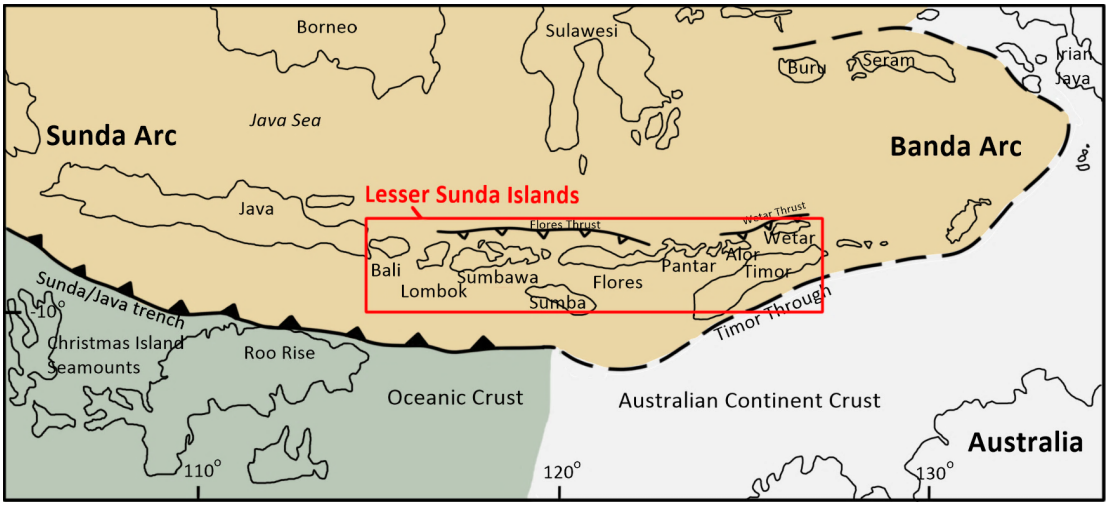

Figure 3. Lesser Sunda Islands between Java and the Banda Arc [2]. The continuity of the trench formed by the subduction of the Indo-Australian Plate under the Eurasian Plate stops at the Sumba Island [16]. That point to the east is influenced by the collision of the Australian Continent with the Banda Arc [16].

3. Sample and Methodology

Well-preserved lava samples were taken from 18 outcrops around Mount Agung (Figure 4). Microscopic observations using a polarizing microscope were conducted on all lava samples to analyze the mineral percentage. Mineral chemistry analysis was carried out on 6 selected samples using Scanning Electron Microscopy-Energy Dispersive X-Ray Spectrometry (SEM-EDS) JEOL JSM-IT-300 of SEM-EDS Laboratory of Chevron-Bandung Insitute of Technology, Indonesia. This test aims to identify the major and minor element content (such as Ti, Al, Fe, Mn, Mg, Ca, Na, K, P, Cr, Ni) of the phenocrysts in the sample. A list of the sample studied in this research is present in Table 1.

As support, geochemical analysis was obtained using published data from Fontjin's [20] and Dempsey's [2] research. Those data are taken from 66 volcanic rock samples (48 samples from [20] and 18 samples from [2]) which consist of major elements (SiO_2, Al_2O_3, Fe_2O_3, FeO, MnO, MgO, CaO, Na_2O, K_2O, TiO_2, P_2O_5) and trace elements (Rb, Sr, Y, Nb, Zr, Cr, Ni, Cu, Zn, Ga, Ba, Pb, Th, U, La, Ce, Nd, Sm). All the supplementary data used in this study are present in Table 2.

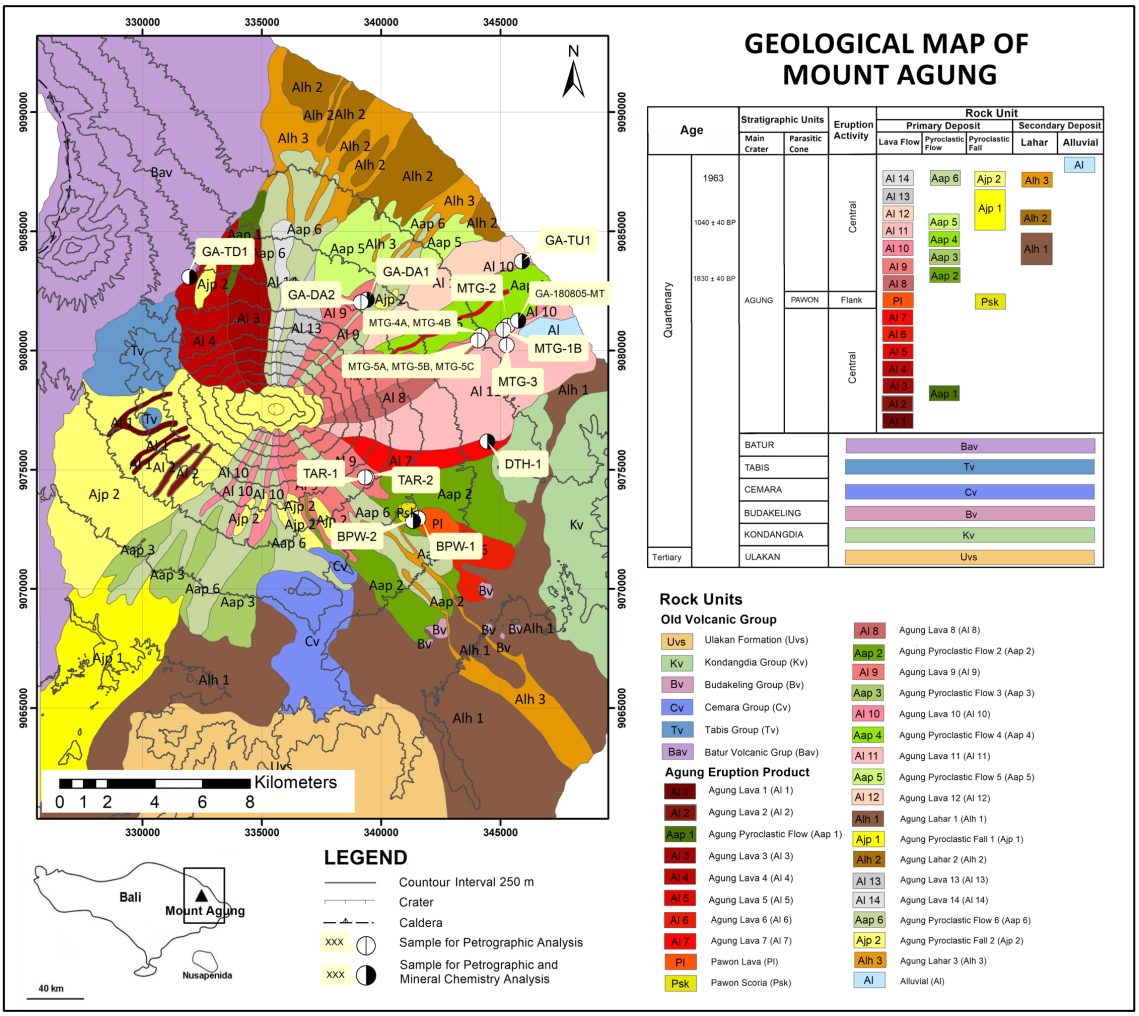

Figure 4. Geological map of the study area [19]. It includes the sample locations used in this study that consist of 18 lava samples for petrographic analysis and 6 of them for mineral chemistry analysis.

Table 1. List of samples used for microscopic observation and mineral chemistry analysis.

Sample Code	Deposit Type	Analysis		Sample Code	Deposit Type	Analysis	
		Petrography	Mineral Chemistry			Petrography	Mineral Chemistry
GA-TU1	Lava	✓	✓	MTG-5C	Lava	✓	
MTG-3	Lava	✓		TAR-1	Lava	✓	
GA-180805-MT	Lava	✓	✓	TAR-2	Lava	✓	
MTG-1B	Lava	✓		GA-DA1	Lava	✓	✓
MTG-2	Lava	✓		GA-DA2	Lava	✓	
MTG-4A	Lava	✓		BPW-1	Lava	✓	
MTG-4B	Lava	✓		BPW-2	Lava	✓	✓
MTG-5A	Lava	✓		DTH-1	Lava	✓	✓
MTG-5B	Lava	✓		GA-TD1	Lava	✓	✓

Table 2. List of samples used as supplementary data in this research for geochemical analysis. It includes rock geochemistry data from published research by Fontjin [20] and Dempsey [2].

Sample Code	Deposit Type	Analysis	Sample Code	Deposit Type	Analysis
		Geochemistry			Geochemistry
Supplementary Data [20]					
AG022A	Lava	✓	AG006bisE	Scoria	✓
AG012I	Scoria	✓	AG006bisF	Ash Fall	✓
AG008B	Pumice	✓	AG006bisH	Ash Fall	✓
AG016C	Scoria	✓	AG021C	Scoria	✓
AG012E	Pyroclastic Flow	✓	AG021D	Ash Fall	✓
AG028B	Pyroclastic Flow	✓	AG021E	Scoria	✓
AG042B	Pyroclastic Flow	✓	AG021H	Ash Fall	✓
AG001bisH	Pumice	✓	AG021I	Scoria	✓
AG045D	Pyroclastic Flow	✓	AG021K	Scoria	✓
AG042D	Pyroclastic Flow	✓	AG006bisO	Scoria	✓
AG001bisB	Pyroclastic Flow	✓	AG006bisS	Scoria	✓
AG042G	Pumice	✓	AG006bisR	Ash Fall	✓
AG001bisC	Scoria	✓	AG006bisT	Scoria	✓
AG001bisE	Pyroclastic Flow	✓	AG006bisK	Scoria	✓
AG042I	Pyroclastic Flow	✓	AG006M	Scoria	✓
AG042bisD	Pyroclastic Flow	✓	AG006N	Scoria	✓
AG042bisB	Pyroclastic Flow	✓	AG006O	Ash Fall	✓
AG024E	Pyroclastic Flow	✓	AG006R	Scoria	✓
AG024D	Pyroclastic Flow	✓	AG006S	Scoria	✓
AG008G	Ash Fall	✓	AG021B	Ash Fall	✓
AG021L	Ash Fall	✓	AG006bisAB	Scoria	✓
AG008I	Scoria	✓	AG006B	Scoria	✓
AG008L	Scoria	✓	AG006F	Scoria	✓
AG006bisC	Scoria	✓	AG024B	Pyroclastic Flow	✓
Supplementary Data [2]					
AG16	Lava	✓	Agu07	Pyroclastic	✓
Agu18	Lava	✓	Agu10	Lava	✓
Agu20	Lava	✓	Agu12	Lava	✓
Agu21	Lava	✓	Agu13	Lava	✓
Agu22	Lava	✓	Agu15	Lava	✓
Agu23	Lava	✓	Agu03	Pyroclastic	✓
Agu24	Lava	✓	Agu30	Lava	✓
Agu25	Pyroclastic	✓	Agu31	Lava	✓
Agu06	Pyroclastic	✓	Agu33	Lava	✓

4. Results

For better understanding, data and stratigraphic correlation were needed to find the connection between all of the existing samples used in this research. The lava samples of Mount Agung eruption were taken from the field based on the division of rock units in Nasution's geological map [19] (Figure. 4). According to the volcano-stratigraphy of Mount Agung, there are 2 dated rock units, Agung Pyroclastic Flow 2 (Aap 2) unit, dated to 1040 ± 40 BP, and Agung Pyroclastic Flow 5 (Aap 5) unit, dated to 1830

± 40 BP. Similar data are also present in Fontjin's research [20]. Sample AG042bisD and AG042bisD have an absolute age of 1040 ± 50 BP, whereas AG006bisE, AG006bisF, and AG006bisH were dated to 1870 ± 40 BP. These two ages become the basis of the sample correlation hypothesis between all the rock units [19] and the absolute age [20] (Figure 5). In addition, these two ages also become the basis for dividing the eruption periods of Mount Agung used in this study.

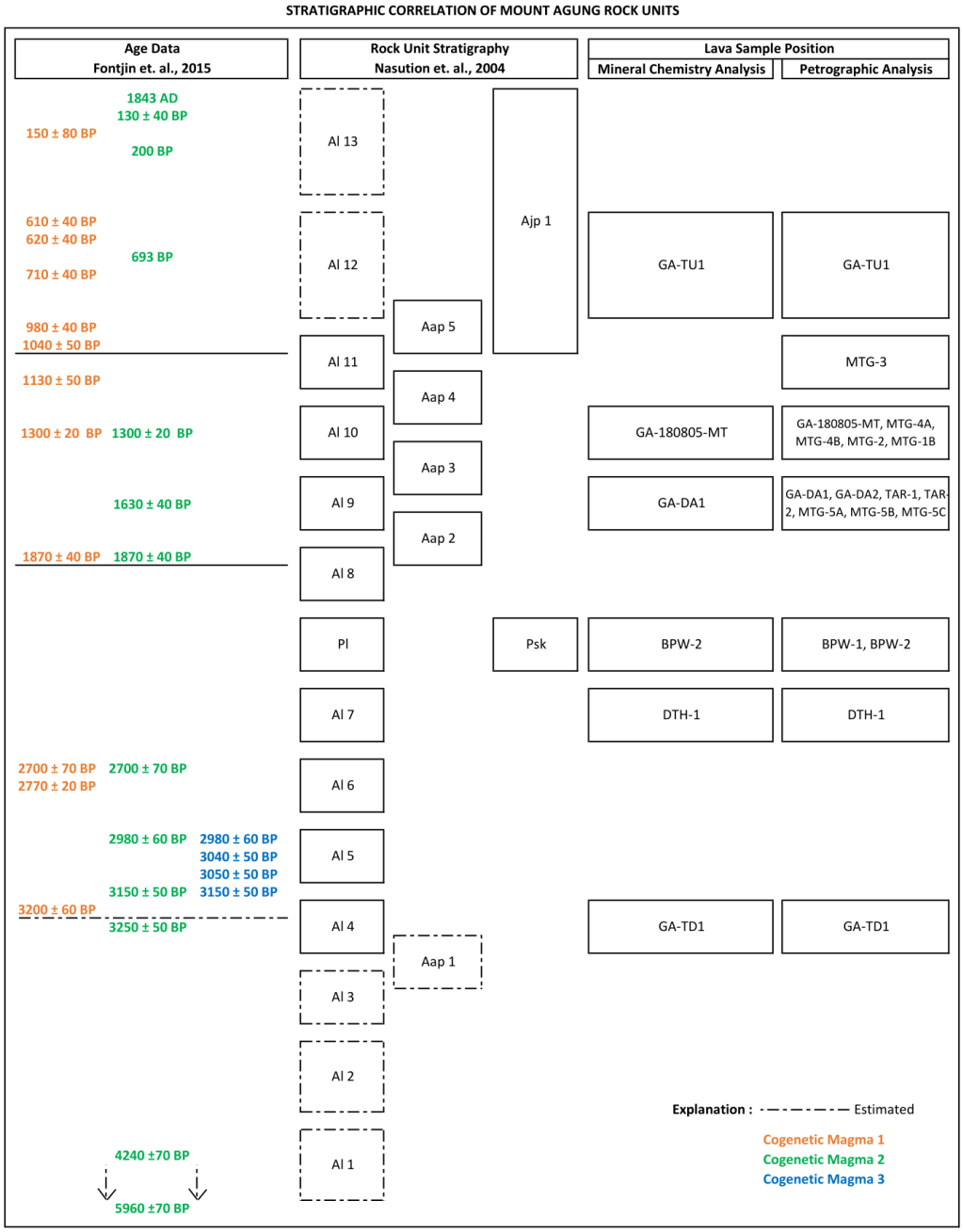

Figure 5. Stratigraphic correlation of age [15], rock units [14], and sample positions representing the rock units used in this study. The cogenetic magma division is obtained based on the sample distribution on the K_2O vs. SiO_2 diagram.

To specify historical activity, the eruption period is detailed using the basis of the geochemistry data plot of Fontjin's [20] and Dempsey's [2] on the K_2O versus SiO_2 diagram, with the assumption K_2O is not affected by the crystal fractionation process. Based on Figure 6, there are three trends of Mount Agung magma differentiation. These trends portray three cogenetic magmas differentiation processes. At the age of 3200 ± 60 BP, there is a sample that has the lowest SiO_2. This sample may be present the closest content of the primitive magma. Rock samples from 3200 ± 60 – 1870 ± 40 BP dominantly had low SiO_2 content. However, rock samples from pre-3200 ± 60 BP had a higher SiO_2. That gives first evidence of the magma evolution process from the pre-3200 ± 60 BP to the 3200 ± 60 – 1870 ± 40 BP period. With those basics, the authors divided Mount Agung's volcanic activity into 4-periods, i.e., the post-1040 ± 50 BP, 1870 ± 40 BP – 1040 ± 50 BP, 3200 ± 60 BP – 1870 ± 40 BP, and the pre-3200 ± 60 BP.

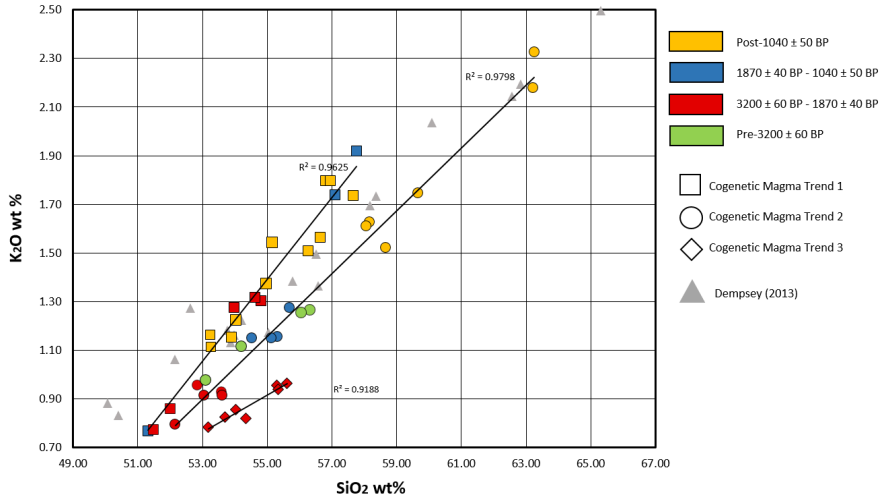

Figure 6. K_2O versus SiO_2 diagram. It shows three cogenetic magma trendlines and the distribution of the samples in every four periods. The data used are from Fontjin's geochemical data [20] and Dempsey's [2] used as a comparison.

4.1. Mineral Composition

Based on microscopic observations of 18 lava samples, all eruption periods produced pyroxene-andesite rocks (name using Williams' classification [21]), which have a porphyritic texture. The phenocrysts contained are dominated by plagioclase, followed by pyroxene, opaque minerals, and olivine.

4.1.1. Plagioclase. Plagioclase is the predominant phenocryst present in all samples. It is found as subhedral crystals that showed varying microtextures. Coarse sieve is abundant followed by glomerocryst, fine sieve, fine-oscillatory zoning, and resorption surface (Figure 7). Based on the An composition [XAn = 100*Ca/(Ca+Na)] taken from mineral chemistry analysis (Figure 8), in pre-3200 ± 60 BP period, plagioclase contains a long-range of $An_{38–89}$. The core tends to be more calcic than the rim. The core's composition is dominant at $An_{70–80}$ and An $_{85–89}$, while the rim's dominant at $An_{50–55}$. In 3200 ± 60 – 1870 ± 40 BP, the An content decreased to $An_{67–83}$. Both core and rim have a wide range of An. In 1870 ± 40 – 1040 ± 50 BP, the An composition generally decreased again to $An_{43–88}$. In the post-1040 ± 50 BP, plagioclase minerals have $An_{38–86}$, with the same distribution pattern as the first period. The core is more calcic than the rim. The core's composition is dominant at $An_{70–85}$, while the rim varies from $An_{35–75}$ but is dominant at $An_{65–70}$. Based on the scanline test, plagioclase has a decreasing percent mass Ca from the core to the rim (normal zoning) (Figure 8).

4.1.2. Pyroxene. Pyroxene minerals as phenocrysts (Figure 9A and 9B) are present in subhedral–anhedral forms. Locally, pyroxenes are found as cumulocrysts along with plagioclase, olivine, and opaque minerals. There are two types of pyroxene observed in each sample, orthopyroxene and

clinopyroxene. Orthopyroxene has enstatite composition, while clinopyroxene has augite composition (classify using [22]). Based on mineral chemistry analysis, In the pre-3200 ± 60 BP period, enstatite has $Mg\#_{61–77}$ [XMg# = 100*Mg/(Mg+Fe^{2+})], whereas augite has $Mg\#_{73–78}$. In the following period, the Mg# content in enstatite generally increased to $Mg\#_{65-76}$, but augite's Mg# decreased to $Mg\#_{71–76}$. In 1870 ± 40 – 1040 ± 50 BP period, the Mg# composition in enstatite and augite generally decrease, to $Mg\#_{65–75}$ and $Mg_{\#72–77}$ in order. However, viewed from the percentage, the pyroxene minerals are more abundant during this period. In the post-1040 ± 50 BP, the Mg# content in enstatite and augite tend to increase, to $Mg\#_{67–72}$ and $Mg\#_{67–81}$. Based on the scanline test, both enstatite and augite have a percent mass of Mg that increases from the core to the rim (Figure 10A and 10B).

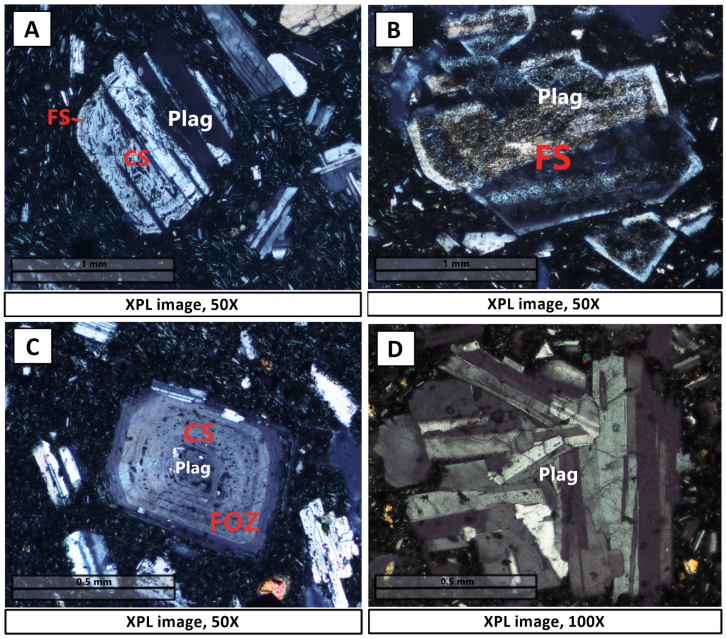

Figure 7. Selected images of optical microscope of plagioclase presented in Mount Agung. (A) Coarse sieve texture in Sample GA-TD1 (pre-3200 ± 60 BP). (B) Fine sieve found in Sample BPW-2 (3200 ± 60 – 1870 ± 40 BP). (C) Fine oscillatory zoning and coarse sieve in Sample TAR-2 (1870 ± 40 – 1040 ± 50 BP). (D) Glomero-crysts found in GA-TU1 (post-1040 ± 50 BP). Detail: Plag = Plagioclase; FS = Fine Sieve; CS = Coarse Sieve; FOZ = Fine Oscillatory Zoning.

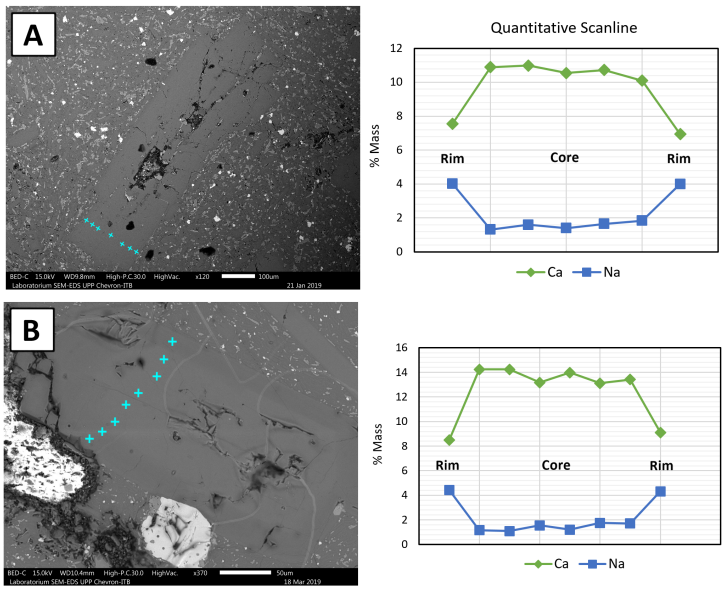

Figure 8. Selected electron images of plagioclase from SEM-EDS mineral chemistry analysis and its quantitative scanline result. Blue +: approximate analyzed points. (A) Plagioclase of Sample GA-TD1 (pre-3200 ± 60 BP period) shows decreasing Ca from the core to the rim. (B) Plagioclase of Sample GA-DA1 (1870 ± 40 – 1040 ± 50 BP) indicates a similar pattern.

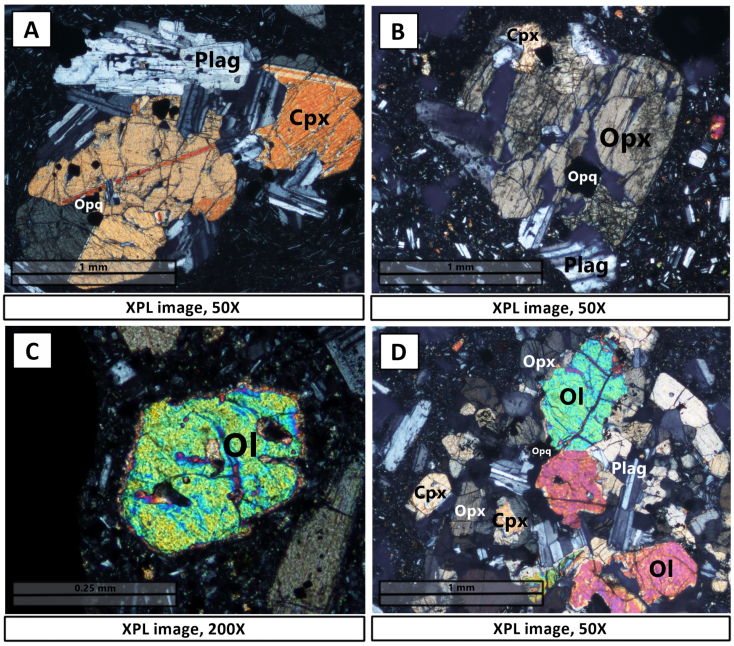

Figure 9. Selected images of optical microscope of minerals presented in the Mount Agung eruption. (A) Clinopyroxene as cumulocrysts of Sample GA-TD1 (pre-3200 ± 60 BP period). (B) Orthopyroxene of Sample BPW-1 (3200 ± 60 – 1870 ± 40 BP). (C) Olivine as microfenocryst in Sample MTG-5A (1870 ± 40 – 1040 ± 50 BP). (D) Olivine, plagioclase, orthopyroxene, clinopyroxene, and opaque minerals cumulocrysts found in Sample MTG-5C (1870 ± 40 – 1040 ± 50 BP). Details: Ol = Olivine; Cpx = Clinopyroxene; Opq = Opaque Mineral; Opx = Orthopyroxene; Plag = Plagioclase.

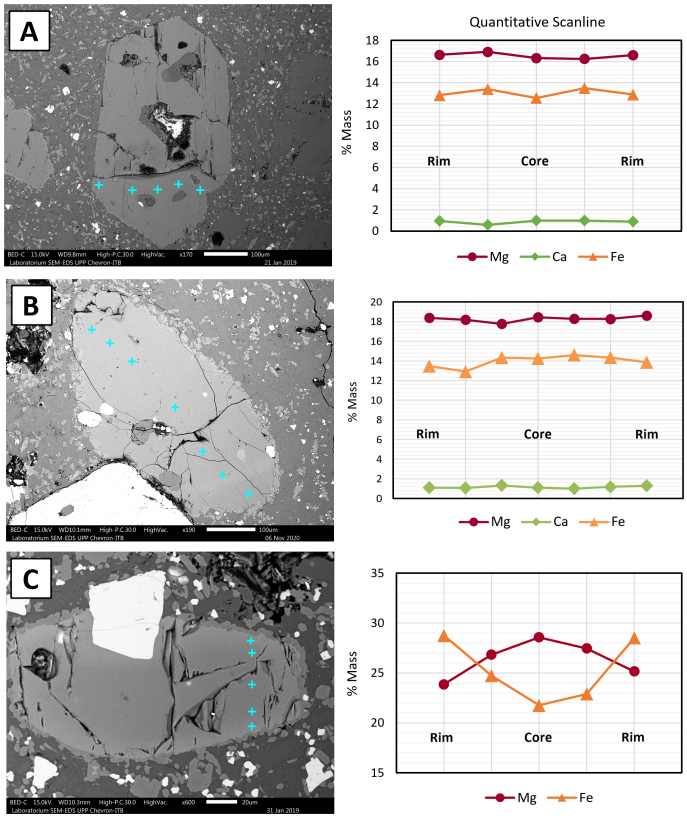

Figure 10. Selected electron images of SEM-EDS mineral chemistry analysis and its quantitative scanline result. Blue +: approximate analyzed points. (A) Enstatite of Sample GA-TD1 (pre-3200 ± 60 BP) generally shows increasing Mg from the core to the rim. (B) Augite of Sample DTH-1 (3200 ± 60 – 1870 ± 40 BP) generally shows increasing Mg from the core to the rim. (C) Olivine with reaction rim of Sample GA-TU1 (post-1040 ± 50 BP) shows decreasing Mg from the core to the rim.

4.1.3. Olivine. Generally, olivine minerals found in all eruption samples are present as microphenocrysts with subhedral–anhedral forms (Figure 9C). Olivine dominantly has a reaction rim composed of pigeonite or enstatite (classify using [22]). Locally, olivine is spotted having a rim that consists of opaque minerals. Based on mineral chemistry analysis, olivine in the pre-3200 ± 60 BP

contains $Fo_{62–78}$ [XFo = 100*Mg/(Mg+Fe)] with a more Mg-rich core than the rim. The core's Fo value is dominant at $Fo_{75–78}$, while the rim is dominant at $Fo_{65–70}$. In 3200 ± 60 – 1870 ± 40 BP, the Fo content tends to decrease, becoming $Fo_{60–71}$, but both core and rim have a wide range of Fo. In 1870 ± 40 – 1040 ± 50 BP period, the Fo content slightly decreased to $Fo_{59–71}$. Locally, olivine is spotted partially oxidized. Then, in the post-1040 ± 50 BP, the Fo composition increase to $Fo_{66–76}$. Olivine percentage is slightly more abundant compared to the previous period. The core is also more Mg-rich than the rim. The core's Fo content is dominant at $Fo_{70–75}$, while the rim is dominant at $Fo_{65–70}$. Based on the scanline test, olivine has a decreasing percent mass of Mg from the core to the rim (normal zoning), which can be caused by the reaction rim (Figure 10C).

4.1.4. Opaque Minerals. Opaque minerals are present as phenocrysts and microphenocrysts with anhedral shapes. Locally, they are found as cumulocrysts along with plagioclase, pyroxene, and olivine (Figure 9D). Based on the mineral chemistry test, the opaque mineral from all eruption periods has a magnetite composition (classify using [23]).

4.2. Geochemical Analysis

Bulk geochemical analysis was carried out using supplementary data from published journals by Fontjin [20]. As a comparison, Dempsey's [2] data was also used in this study, especially to see the data clusters distribution suitability.

4.2.1. Normative Minerals. Normative minerals are the number of minerals present in the norm expressed as their molecular proportion [24]. This paper used the CIPW calculation excel sheet program written by Hollocher [25]. Based on Table 3, all samples from each period are characterized by the presence of quartz and hypersthene that shows saturated to highly saturated silica magma. Hypersthene minerals are found the highest in 3200 ± 60 – 1870 ± 40 BP and 1870 ± 40 – 1040 ± 50 BP. However, the quartz in 1870 ± 40 – 1040 ± 50 BP is slightly higher. It suggests that the magma saturation level reach the lowest in 3200 ± 60 – 1870 ± 40 BP. The quartz minerals are most abundant in the youngest period which implies that the silica saturation in magma is on the highest level compared to the other periods.

Table 3. Percentage of normative minerals present in each period of Mount Agung eruption. The data used are geochemistry data of Fontjin [20].

Eruption Period	Pre-3200 ± 60 BP	3200 ± 60 – 1870 ± 40 BP	1870 ± 40 – 1040 ± 50 BP	Post-1040 ± 50 BP
Deposite Type	Scoria, Pyroclastic Flow	Scoria, Ash Fall	Scoria, Ash Fall, Pyroclastic Flow	Pyroclastic Flow, Pumice, Scoria, Ash
Normative Minerals (wt%)				
Quartz	2.92 - 6.34	1.35 - 6.92	0.39 - 8.26	2.76 - 15.57
Plagioclase	59.99 - 67.66	56.61 - 72.14	55.35 - 68.3	55.1 - 59.82
Orthoclase	5.73 - 7.45	4.61 - 7.68	4.55 - 11.46	6.68 - 10.7
Corundum	0	0 - 0.64	0	0
Diopside	1.22 - 6.66	0 - 8.36	3.13 - 6.43	0.52 - 8.49
Hypersthene	13.85 - 21.34	13.53 - 24.61	13.66 - 25.49	10.48 - 19.98
Ilmenite	1.44 - 2.07	1.42 - 2.22	1.58 - 2.03	1.12 - 1.73
Magnetite	1.09 - 1.59	1.07 - 1.83	1.15 - 1.59	0.87 - 1.48
Apatite	0.53 - 0.65	0.35 - 0.65	0.37 - 0.65	0.53 - 0.63
Zircon	0.01	0.01	0.01 - 0.03	0.01 - 0.03

4.2.2. Rock Classification. Eruption product is a good indicator for determining the origin magma content. Using plotted data on Le Bas diagram [26] of total alkali ($Na_2O + K_2O$) against SiO_2 (Figure 11), the eruption products from each period are as follows: (1) The pre-3200 ± 60 BP consist of basaltic-

andesite rocks with SiO_2 53 – 56 wt%; (2) 3200 ± 60 – 1870 ± 40 BP consists of basalt to basaltic-andesite rocks with SiO_2 51 – 56 wt%; (3) 1870 ± 40 – 1040 ± 50 BP consists of basalt to andesite rocks with SiO_2 53 – 58 wt%, but more dominantly in SiO_2 51 – 58%; (4) The post-1040 ± 50 BP consists of basaltic-andesite to dacite rocks with SiO_2 53 – 63% wt%.

4.2.3. Magma Affinity. Magma series or magma affinity can interpret the volcano-tectonic setting [11]. The magma affinity is obtained by plotting the geochemical data on the K_2O vs. SiO_2 [27]. The data plot result (Figure 12) shows that all samples are from the calc-alkaline magma series. According to Wilson [11], it is a feature of convergent plate boundaries (subduction).

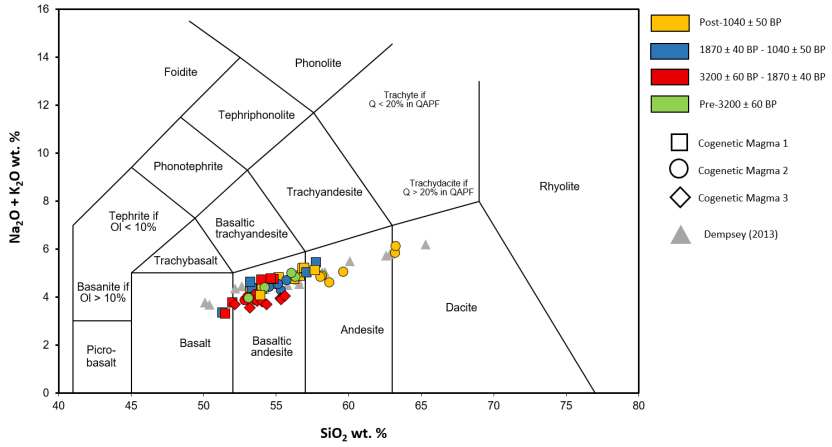

Figure 11. The result of Fontjin's data [20] plotting on the $Na_2O + K_2O$ vs. SiO_2 diagram [26] which determines the geochemical rock name. Dempsey's data [2] is used as a comparison.

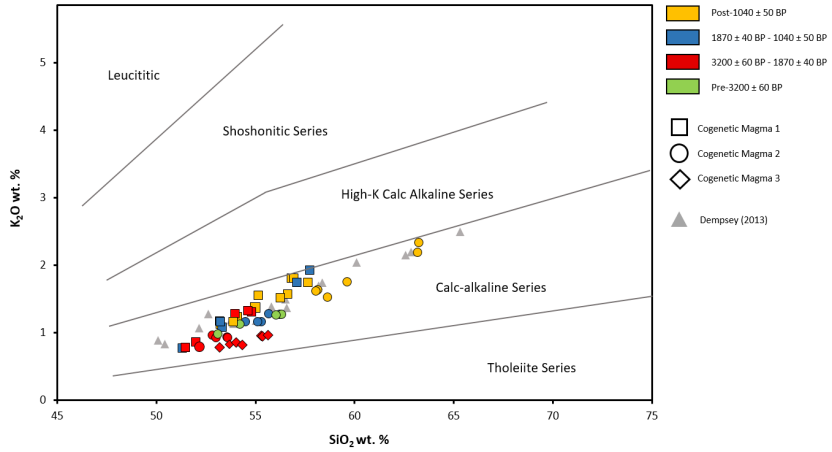

Figure 12. Distribution of Fontjin's data [20] on the K_2O vs. SiO_2 diagram [27] which indicates the magma series of Mount Agung eruption products. Dempsey's data [2] is used as a comparison.

4.2.4. Harker Diagram and Crystal Fractionation. Harker diagrams show the change of major elements to SiO_2 [28, 29]. This diagram can provide magmatic activity interpretation, which includes the evolution and magma differentiation. Crystal fractionation is characterized by a curved pattern due to the depletion of certain compatible elements from the magma solution that depends on the mineral phase undergoing crystallization [30]. Based on Figure 13, crystal fractionation occurred during Mount Agung's magma differentiation. It represents from the TiO_2, MgO, Fe_2O_3, and CaO diagrams. In the TiO_2 diagram, the steep gradient in the older period (pre-1040 ± 50 BP) indicates the fractionation of magnetite. The MgO and Fe_2O_3 diagrams show the fractionation of olivine and/or pyroxene, which is also predominant in the older period (pre-1040 ± 50 BP). Next, the CaO diagram exhibits the plagioclase

fractionation, and compared to other minerals, it predominantly happened in the younger period (post-1040 ± 50 BP) instead.

Crystal fractionation can also be seen from the log K_2O against the log Zr/Nb diagram [2] (Figure 14). Based on the previous Harker Diagram, there are differences in the minerals undergoing fractionation. This interpretation is also supported by Dempsey's research [2], which stated that there are two fractionation vectors during the magma differentiation process. The cause can be identified from plagioclase minerals. During the differentiation process, plagioclase fractionation can be temporarily suspended if the magma is under high-pressure conditions or has a high water content [2, 31]. Figure 15 shows data distribution against the two trendlines of plagioclase fractionation [31]. It can be seen that the pre-3200 ± 60 BP, 3200 ± 60 – 1870 ± 40 BP, and 1870 ± 40 – 1040 ± 50 BP periods, in general, followed the curved line indicating that the plagioclase fractionation was restrained. In contrast, the post-1040 ± 50 BP period, in general, followed the other line that shows the occurrence of plagioclase fractionation. These differences correspond to Dempsey [2] and Geiger [32], which said that Mount Agung is possibly controlled by the presence of a high pressure-deep magma reservoir that can withstand plagioclase fractionation and also a shallow magma reservoir with lower pressure.

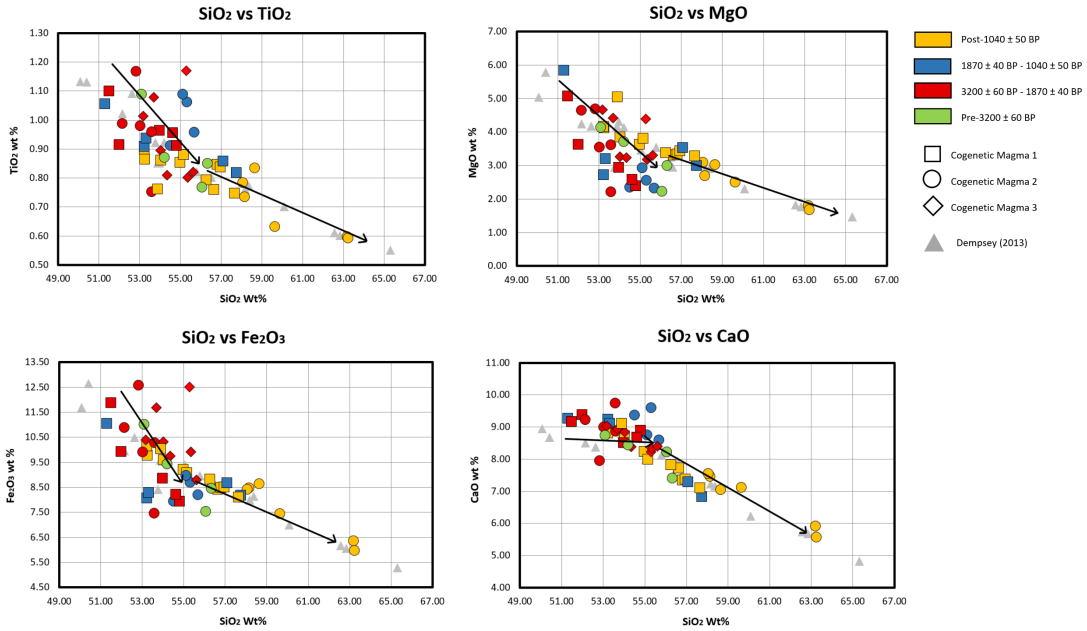

Figure 13. Selected Harker diagrams show the distribution of the major elements using the SiO_2 as a differentiation index. The black arrow indicates the trend of certain minerals depletion. The geochemistry data plotted is from Fontjin [20] and Dempsey's data [2] is used as a comparison.

4.2.5. Spider Diagram and Trace Element. Discovering the tectonic setting can be done by plotting trace elements that have been normalized with the primitive mantle onto a spider diagram [33]. Normalization is used to eliminate the Oddo-Harkins effect on the graph. From Figure 16, it can be seen that the Rb, Ba, Th, and K (LILE) and La – Sm (LREE) contents are enriched, while Eu – Lu (HREE) experienced depletion. According to Dirk [34], these features indicate the properties of a subduction zone. In addition, the Nb content also shows a negative anomaly which is also a characteristic of convergent plate boundaries [11]. Thus, it can be inferred that Mount Agung comes from a volcanic associated with a convergent plate boundary (subduction).

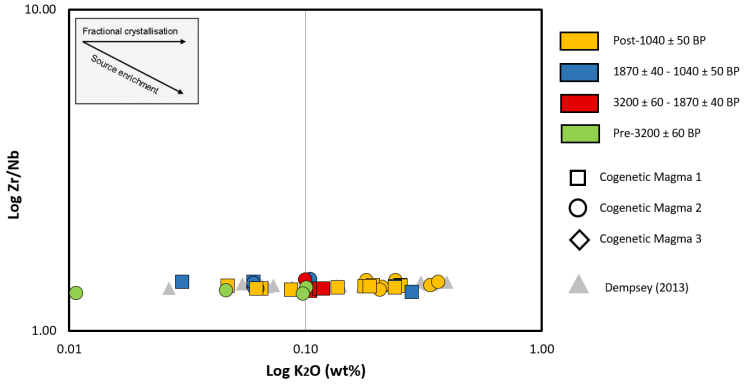

Figure 14. Diagram of log K_2O log vs log Zr/Nb which distinguishes crystal fractionation with primitive mantle enrichment [2]. The rock geochemistry data used is Fontjin's [20] with Dempsey's data [2] as a comparison.

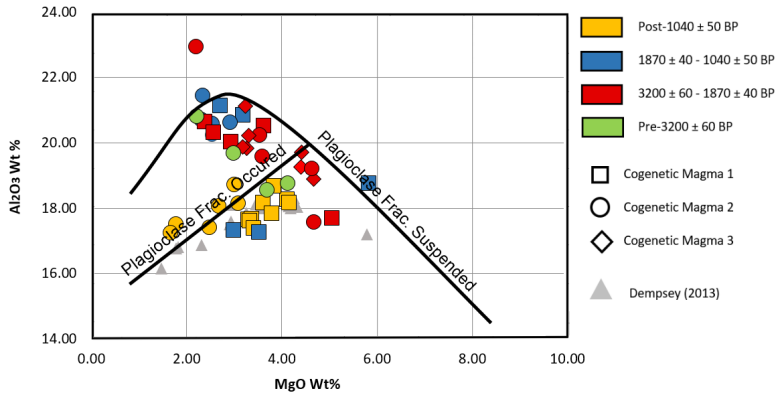

Figure 15. Diagram of MgO against Al_2O_3 with two trends of plagioclase fractionation [2, 31]. The geochemistry data used is from Fontjin [20] with Dempsey's data [2] as a comparison.

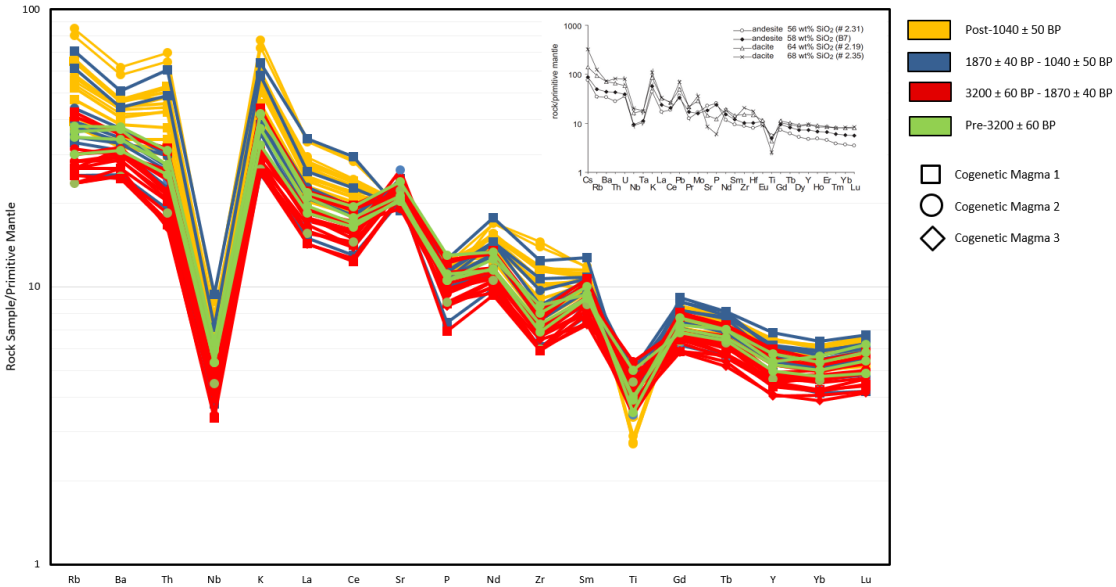

Figure 16. Spider diagram of Mount Agung eruption trace elements. The rock geochemistry data comes from Fontjin [20]. The sample was normalized against the primitive mantle [32]. A similar diagram of the Mount Batur eruption products [35] was used as a comparison.

There are two types of subduction, island arcs and active continental margins [11]. Those two types can be distinguished using the ratio of Zr to Zr/Y from the Pearce [36]. Based on Figure 17, Mount Agung originates from the subduction of oceanic crust beneath continental crust. Next, the La/Sm to Th/Nb diagram can specify the differentiation type influenced by its tectonic setting [37, 38]. Figure 18 shows that in the older period (pre-1040 ± 50 BP), the magma differentiation process is subduction-related enrichment. Whereas in the younger period (post-1040 ± 50 BP), there may be a slight influence from the presence of crustal contamination.

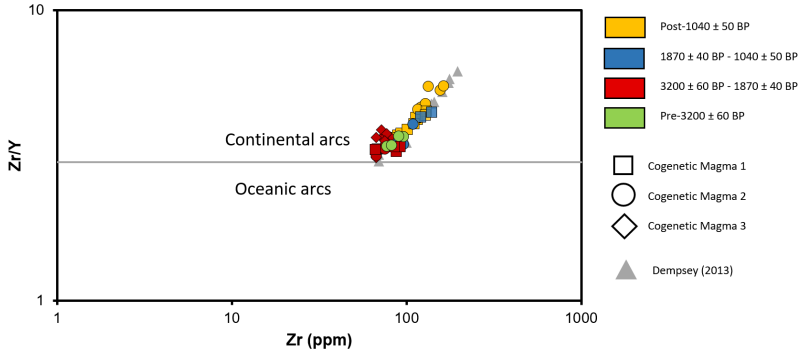

Figure 17. Diagram of Zr vs. Zr/Y which differentiate continental and oceanic arc [36]. The rock geochemistry data is from Fontjin [20]. Dempsey's data [2] is used as a comparison.

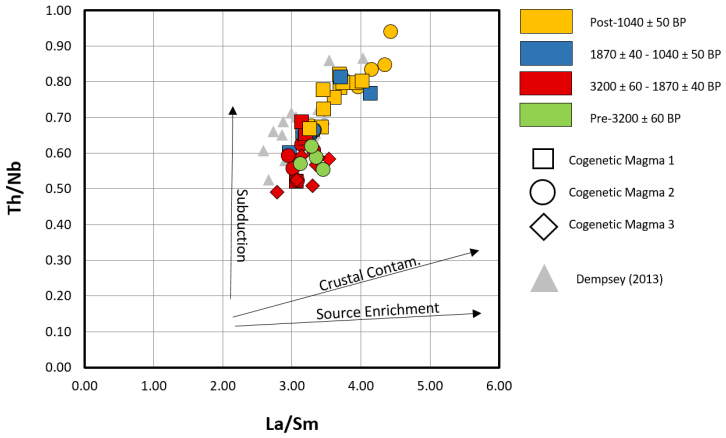

Figure 18. La/Sm vs. Th/Nb diagram with several differentiation vectors [37, 38]. The rock geochemistry data is from Fontjin [20]. Dempsey's data [2] is used as a comparison.

5. Discussion

5.1. Nature of Primitive Magma Source

Magma source interpretation of Mount Agung can be acquired by looking at the Fo content in olivine phenocrysts [39]. Magma originating directly from the mantle source has fosterite content more than Fo_{88} [11, 40]. The Fo in olivine from Mount Agung eruption ranged from $Fo_{60–78}$. It proves that the primitive magma of Mount Agung originates from the partial melting process instead. The SiO_2 content of the primitive magma of Mount Agung can be interpreted from the plot diagram of K_2O against SiO_2 (Figure 6), assuming that the K_2O content is not affected by the crystal fractionation process and can represent the actual content of the magma. Based on the diagram, three trendlines come from one point at lower SiO_2. Therefore, it indicates that the three cogenetic magmas may originate from the same source. By extending the trendline, the primitive magma has a SiO_2 content of ~50 wt%.

5.2. Magma Chamber Condition

Plagioclase minerals, mentioned in several studies, may be an efficient tool for understanding the dynamic magmatic process due to their high sensitivity to temperature-pressure (T-P) conditions, water content, and melt composition changes [41, 42, 43, 44]. The wide range of cores and diversity in An zoning imply a compositional change of host magma or change in the crystallization conditions that suggest a diverse magma chamber system [44]. Based on mineral chemical analysis, Mount Agung eruption produces a wide range of An zoning, ~$An_{38–89}$. As stated in the previous Harker diagram and crystal fractionation analysis, Mount Agung is possibly controlled by the presence of a deep and shallow magma chamber [2, 32, 45]. The deep high-temperature magma chamber feeds basaltic magma to the shallower lower-temperature magma chamber [43]. During this process, decompression, heat addition, magma mixing, rapid undercooling, or magma mixing may occur simultaneously [43]. Thus, these processes will produce disequilibrium plagioclase microtextures, such as zoned, sieved (coarse and fine sieve), and dissolved (rounded zone, resorption surface) phenocryst [43] that are all present in every period of Mount Agung eruption.

5.3. Tectonic Implication

The results of this study suggest that Bali Island is interpreted as having a basement that supports the recent studies about the distribution of continental blocks and fragments in SE Asia including Sundaland [7, 8]. Our research found that Bali is underlain by continental crust. This is shown from the Zr vs. Zr/Y diagram indicated that Bali was formed as a result of the continental arc or active continental margin. It is different from previous research [5, 9, 10], which says that Bali was formed due to island arcs or as known as having the oceanic basement. The distinctive feature of island arcs generally is a linear or arcuate chain of small islands [11], which in this case is the Lesser Sunda Islands. The active continental margin, on the other hand, is broadly similar to the island arc, although the passage of magma through the thick continental crust added complexities [11]. This case is not found in Bali, because the crust underlain this island is micro-continent, which may be derived from the Australian continent and suture zone [4, 16].

The formation of Bali Island was deducted in the reconstruction of the Southeast Asian tectonic model [4]. Approximately 15 million years ago, the subduction of the Indian Ocean with Eurasia caused the Australian continent to dock with Sundaland, resulting in the formation of a suture zone [4] (Figure 2). Then, this subduction event generated partial melting, which became the source of volcanic arc magma whose eruptions then slowly formed Bali Island as it is now. This can be proven by the oldest deposits that form Bali Island, the early Miocene Ulakan formation, which is a volcanic rock deposit [17, 18]. The volcanic arc activity was divided into three cycles, i.e., the first cycle occurred in the Miocene, the second cycle occurred in the late Pliocene which was marked by the appearance of more alkaline lava, and the third cycle occurred in the quarternary period [14]. The last cycle formed several volcanoes in Bali and one of them is Mount Agung.

Based on the magma evolution of Mount Agung in each period, it can be seen that the K_2O and SiO_2 content in magma is generally increasing. This development, seen from the major element diagrams, was caused by magma differentiation in the form of crystal fractionation of olivine-pyroxene-magnetite (pre-1040 ± 50 BP) while the younger period was in the form of plagioclase fractionation. However, in the post-1040 ± 50 BP period, crystal fractionation was not the only differentiation process that happened. There was also crustal contamination, which is shown from the La/Sm and Th/Nb trace element diagrams (Figure 18). Based on the spider diagram (Figure 16), post-1040 ± 50 BP also has a higher trace element content of K, Sr, Ba, Zr, and Th than in other periods. It also suggests that crustal involvement [11] indeed took place in the younger period. Lesser Sunda Island, where Bali resides, coincides with a change in the plate convergence type from subduction to collision [16]. This intimates that the Lesser Sunda Islands are slowly will more likely to become affected by the collision of the Australian continent with the Banda arc, which may explain why the continental crust influence is greater in the younger period.

6. Conclusion

From the result and discussion, it can be concluded that:
(1) Mount Agung's primitive magma originated from partial melting and it has approximately 50 wt% of SiO_2 content. This magma underwent a differentiation process in multiple magma chambers.
(2) The tectonic setting of Bali Island is an active continental margin. The trace element analysis confirms that Bali Island has a continental basement, which is more precisely a micro-continent basement and this confirms the recent studies of Sundaland [7, 8]. This evidence suggests that Bali Island is still included in Sundaland and may be part of its eastern boundary.

References

[1] Hall R and Smyth H 2008 Cenozoic arc processes in Indonesia: identification of the key influences on the stratigraphic record in active volcanic arcs *Geol. Soc. of America Special Pub* **436** 27–54
[2] Dempsey S R 2013 Geochemistry of volcanic rocks from the Sunda Arc *Ph.D. Thesis Durham University*
[3] Tregoning P, Brunner F K, Bock Y, Puntodewo S S, McCaffrey R, and Genrich J F, Calais E, Rais J, and Subarya C 1994 First geodetic measurement of convergence across the Java Trench *Geophys. Research Letters* **21** 19 2135–2138
[4] Hall R and Sevastjanova I 2012 Australian crust in Indonesia *Australian J of Earth Sci* **59** 827–844
[5] Hamilton W 1973 Tectonics of the Indonesian region *Geol. Soc. Malaysia* **6** 3–10
[6] Wheller G E 1986 Petrogenesis of Batur caldera, Bali, and the geochemistry of Sunda-Banda arc basalts *Ph.D. thesis University of Tasmania*
[7] Hall R 2014 The origin of Sundaland, *Proc. of Sundaland Resources MGEI Annual Conv.* (Indonesia)
[8] Metcalfe I 2017 Tectonic evolution of Sundaland *Bul. of the Geol. Soc. of Malaysia* **63** 27–60
[9] Katili J A 1975 Volcanism and plate tectonic in Indonesian island arcs *Tectonophysics* **26** 165–188
[10] Purwandono A F, Bonte D, Utami P, Pramumijoyo S, Harijoko A, Beekman F, and van Wees J D 2019 Tectonic and compositional variation in Flores Island, Indonesia: implication for volcanic structure and geothermal occurrences *European Geothermal Cong.* (Netherland)
[11] Wilson M 1989 *Igneous Petrogenesis A Global Tectonic Approach* (Netherland: Springer)
[12] Pearce J A and Cann J R 1973 Tectonic setting of basic volcanic rocks determined using trace element analyses *Earth and Planetary Sci. Letter* **19** 290–300
[13] Wibowo B, Mellawati J, and Susiati H 2011 Kajian evolusi geokimia dan kaitannya dengan tingkat bahaya Aunung Api Muria terhadap Tapak PLTN Muria *Jurnal Pengembangan Energi Nuklir* **13** 1
[14] van Bemmelen R W V 1949 *The Geology of Indonesia (General Geology of Indonesia and Adjacent Archipelagoes)* vol. 1A (The Hague: Government Printing Office)
[15] Hutchison C S 2007 *Geological Evolution of South-East Asia 2nd Edition* (Malaysia: Geological Society of Malaysia)
[16] Minarwan 2012 Tectonic models of the Lesser Sunda Islands *Berita Sedimentologi* **25** 8–15.
[17] Purbo-Hadiwidjojo M 1972 The geologic map of Bali, Indonesia, scale 1:250.000 *Geol. Survey of Indonesia*
[18] Sutawidjaja I S 2009 Ignimbrite analyses of Batur Caldera, Bali, based on ^{14}C dating *Jurnal Geologi Indonesia* **4** 3 189–202
[19] Nasution A, Haerani N, Mulyadi D, and Hendrasto M 2004 Peta Geologi Gunungapi Agung, Bali, Skala 1 : 50.000 *Direktorat Vulkanologi dan Mitigasi Bencana Geologi*
[20] Fontijn K, Costa F, Sutawidjaja I, Newhall C G, and Harrin J S 2015 A 5000-year record of multiple highly explosive mafic eruptions from Gunung Agung (Bali, Indonesia): implications

for eruption frequency and volcanic hazards *Bull Volcanol* **77** 59.
[21] Williams H, Turner F J, dan Gilbert C M 1982 *Petrography: An Introduction to the Study of Rocks in Thin Section 2nd edition* (San Fransisco: W. H. Freeman and Company)
[22] Morimoto N, Fabries J, Fergusson A K, Guizbourg I D, Ross M, Seifert F A, Zussman J, Aoki K, and Gottardi G 1988 Nomenclature of pyroxenes *American Mineralogist* **73** 1123–1133
[23] Buddington A F and Lindsley D H 1964 Iron-titanium oxide minerals and synthetic equivalents. *J. Petrol.* **5** 210–357
[24] Kelsey C H 1965 Calculation of the CIPW norm *Mineralogical Mag.* **34** 276–282
[25] Hollocher K 2004 CIPW norm calculation program *Geology Department Union College*
[26] Le Bas M J, Le Maitre R W, Streckeisen A L, and Zanettin B 1986 A classification of volcanic rock based on the total alkali-silica diagram *J. of Petrology* **27** 745–50
[27] Peccerrillo R and Taylor S R 1976 Geochemistry of Eocene calc-alkaline volcanic rocks from the Kastamonu Area, Northen Turkey *Contribution to Mineralogy and Petrololgy* **58** 63–81
[28] Harker A 1909 *The Natural History of Igneous Rocks* (London: Methuen and Co.)
[29] Winter J D 2014 *Principles of Igneous and Metamorpfic Petrology Second Edition* (America: Pearson New International Edition/Pearson Educational Limited)
[30] Novak S W and Bacon C R 1986 Pliocene volcanic rocks of the Coso Range, Inyo County, California *U.S. Geol. Survey Prof. Paper* 1383
[31] Parman S W, Grove T L, Kelley K A, and Plank T 2011 Along-Arc variations in the pre-eruptive H_2O contents of Mariana Arc magmas inferred from fractionation paths *J. of Petrology* **52** 2 257–278
[32] Geiger H, Troll V R, Jolis E M, Deegan F M, Harris C, Hilton D R, and Freda C 2018 Multi-level magma plumbing at Agung and Batur volcanoes increases risk of hazardous eruption *Sci. Reports* **8** 10547
[33] Sun S S, and McDonough W F 1989 Chemical and Isotope Systematics of Oceanic Basalts: implications for mantle composition and processes, magmatism in ocean basins *Geol. Soc. of London* **42** 313–345
[34] Dirk M H J 2008 Petrologi-geokimia batuan Gunung Api Tampomas dan sekitarnya *Pusat Survei Geologi Jurnal Geologi Indonesia* **3** 1 23–35
[35] Reubi O I and Nicholls A 2005 Structure and dynamics of a silicic magmatic system associated with caldera-forming eruptions at Batur Volcanic Field, Bali, Indonesia *J. of Petrology* **46** 7
[36] Pearce J A 1983 *Role of the sub-continental lithosphere in magma genesis at active continental margins* (Chesire: Shiva Publications) p 230–249
[37] Plank T 2005 Constraints from thorium/lanthanum on sediment recycling at subduction zones and the evolution of the continents *J. of Petrology* **46** 921–944
[38] Barresi T, Nelson J L, Dostal J. and Friedman R 2015 Evolution of the Hazelton arc near Terrace, British Columbia: stratigraphic, geochronological, and geochemical constraints on a Late Triassic – Early Jurassic arc and Cu–Au porphyry belt *Can. J. Earth Sci* **52** 466–494
[39] Rogkala A, Petrounias P, Tsikouras B, Giannakopoulou P P, and Hatzipanagiotou K 2019 Mineralogical evidence for partial melting and melt-rock interaction processes in the mantle peridotites of Edessa Ophiolite (North Greece) *Minerals* **9** 120
[40] Arai S 1994 Characterization of spinel peridotites by olivine-spinel compositional relationship: review and interpretation *Chem. Geol.* **113** 191–204
[41] Ginibre C, Wörner G, and Kronz A 2002 Minor- and trace-element zoning in plagioclase: implications for magma chamber processes at Parinacota volcano, northern Chile *Cont. to Mineralogy and Petrology* **143** 300–315
[42] Ginibre C and Wörner G 2007 Variable parent magmas and recharge regimes of the Parinacota magma system (N. Chile) revealed by Fe, Mg and Sr zoning in plagioclase *Lithos* **98** 118–140.
[43] Renjith M L 2014 Micro-textures in plagioclase from 1994-1995 eruption, Barren Island Volcano: Evidence of dynamic magma plumbing system in the Andaman subduction zone *Geosci. Frontiers* **5** 113–126.

[44] Aaltonen M 2018 Crustal contamination recorded by zoned plagioclase in primitive Karoo flood basalts, Luenha River, Mozambique *Master's thesis University of Helsinki*
[45] Syahbana D K, Kasbani K, Suantika G, Prambada O, Andreas A S, Saing U B, Kunrat L, Andreastuti S, Martanto M, Kriswati E, Suparman Y, Humaida H, Ogburn S, Kelly P J, Wellik J, Wright H M N, Pesicek J D, Wessels R, Kern C, Lisowski M, Diefenbach A, Poland M, Beauducel F, Pallister J, Vaughan J D, and Lowenstern J B 2019 The 2017–19 activity at Mount Agung in Bali (Indonesia): intense unrest, monitoring, crisis response, evacuation, and eruption *Scientific Reports* **9** 8848

Acknowledgments
This research is part of Penelitian, Pengabdian Masyarakat, dan Inovasi (PPMI) Institut Teknologi Bandung 2021. The fieldwork was partially supported by the USAID's PEER (Partnership for Enhance Engagement in Research) program with agreement number AID-OAA-A-11-00012.